View metadata, citation and similar papers at core.ac.uk
brought to you by 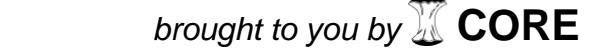
provided by AFTI Scholar (Air Force Institute of Technology)

Air Force Institute of Technology
AFIT Scholar

Faculty Publications

5-2019

Band-to-band Transitions and Critical Points in the Near-infrared to Vacuum Ultraviolet Dielectric Functions of Single Crystal Urania and Thoria

Alyssa Mock

Christina L. Dugan

Sean Knight

Rafał Korlacki

J. Matthew Mann

See next page for additional authors

Follow this and additional works at: https://scholar.afit.edu/facpub

Part of the Atomic, Molecular and Optical Physics Commons

Recommended Citation
A. Mock, C.L. Dugan, S. Knight, R. Korlacki, J.M. Mann, M.M. Kimani, J.C. Petrosky, P.A. Dowben, and M. Schubert, Appl. Phys. Lett. 114, 211901 (2019). https://doi.org/10.1063/1.5087059

This Article is brought to you for free and open access by AFIT Scholar. It has been accepted for inclusion in Faculty Publications by an authorized administrator of AFIT Scholar. For more information, please contact richard.mansfield@afit.edu.

Authors
Alyssa Mock, Christina L. Dugan, Sean Knight, Rafał Korlacki, J. Matthew Mann, Martin M. Kimani, James C. Petrosky, Peter A. Dowben, and Mathias Schubert

This article is available at AFIT Scholar: https://scholar.afit.edu/facpub/579

Applied Physics Letters

Band-to-band transitions and critical points in the near-infrared to vacuum ultraviolet dielectric functions of single crystal urania and thoria

Cite as: Appl. Phys. Lett. **114**, 211901 (2019); https://doi.org/10.1063/1.5087059
Submitted: 27 December 2018 . Accepted: 06 May 2019 . Published Online: 29 May 2019

Alyssa Mock, Christina Dugan, Sean Knight, Rafał Korlacki, J. Matthew Mann, Martin M. Kimani, James C. Petrosky, Peter A. Dowben, and Mathias Schubert

View Online
Export Citation
CrossMark

ARTICLES YOU MAY BE INTERESTED IN

Upper limit for angular compounding speckle reduction
Applied Physics Letters **114**, 211101 (2019); https://doi.org/10.1063/1.5088709

Spin-on-diffussants for doping in transition metal dichalcogenide semiconductors
Applied Physics Letters **114**, 212102 (2019); https://doi.org/10.1063/1.5091553

Effect of thickness on metal to semiconductor transition in La doped $BaSnO_3$ films deposited on high mismatch LSAT substrates
Applied Physics Letters **114**, 212103 (2019); https://doi.org/10.1063/1.5082944

Meet the Next Generation of Quantum Analyzers
And Join the Launch Event on November 17th

Applied Physics Letters ARTICLE scitation.org/journal/apl

Band-to-band transitions and critical points in the near-infrared to vacuum ultraviolet dielectric functions of single crystal urania and thoria

Cite as: Appl. Phys. Lett. **114**, 211901 (2019); doi: 10.1063/1.5087059
Submitted: 27 December 2018 · Accepted: 6 May 2019 ·
Published Online: 29 May 2019

View Online

Export Citation

CrossMark

Alyssa Mock,[1,2,a] Christina Dugan,[3,b] Sean Knight,[1,c] Rafał Korlacki,[1,d] J. Matthew Mann,[4,e] Martin M. Kimani,[4,5,f] James C. Petrosky,[3,g] Peter A. Dowben,[6,h] and Mathias Schubert[1,2,7,i]

AFFILIATIONS

[1]Department of Electrical and Computer Engineering, University of Nebraska-Lincoln, Lincoln, Nebraska 68588, USA
[2]Terahertz Materials Analysis Center, Department of Physics, Chemistry and Biology (IFM), Linköping University, SE 58183 Linköping, Sweden
[3]Air Force Institute of Technology, Wright-Patterson Air Force Base, Ohio 45433-7765, USA
[4]Air Force Research Laboratory, Sensors Directorate, Wright Patterson AFB, Ohio 45433, USA
[5]KBRwyle, Dayton, Ohio 45431, USA
[6]Department of Physics and Astronomy, University of Nebraska-Lincoln, Theodore Jorgensen Hall, 855 North 16th Street, Lincoln, Nebraska 68588-0299, USA
[7]Leibniz Institute for Polymer Research, 01069 Dresden, Germany

[a]Electronic mail: amock@huskers.unl.edu
[b]Electronic mail: christina.l.dugan.mil@mail.mil
[c]Electronic mail: sean.knight@engr.unl.edu
[d]Electronic mail: rkorlacki2@unl.edu
[e]Electronic mail: james.mann.11@us.af.mil
[f]Electronic mail: Martin.Kimani@fda.hhs.gov
[g]Electronic mail: James.Petrosky@afit.edu
[h]Electronic mail: pdowben@unl.edu
[i]Electronic mail: schubert@engr.unl.edu

ABSTRACT

Band-to-band transition energy parameters for single-crystal actinide samples of uranium oxide and thorium oxide were determined and compared using spectroscopic ellipsometry and critical-point dielectric function analyses. Spectroscopic ellipsometry measurements from the near-infrared to the vacuum ultraviolet spectral region were used to determine the dielectric functions of uranium oxide and thorium oxide. The critical-point structure is similar between UO_2 and ThO_2 but strongly blue shifted for ThO_2. We find bandgap energies of 2.1 eV and 5.4 eV for UO_2 and ThO_2, respectively.

https://doi.org/10.1063/1.5087059

Uranium dioxide (urania), UO_2, and thorium dioxide (thoria), ThO_2, have garnered interest recently as semiconductors suitable for neutron detection.[1,2] Present knowledge of the electronic and optical properties of ThO_2 is scarce. Knowledge for UO_2 is also not exhaustive. Until recently, experimental studies of optical and electronic properties of UO_2 and ThO_2 have been limited due to the nonavailability of single-crystal samples of optical quality. Our previous research on these samples indicates high-quality ordered structures of near stoichiometric UO_2 as indicated by core level photoemission spectroscopy and other techniques[3–7] and compared to previous measurements of growth by other processes.[8] This study is a continuation of the previous work given that we have evidence that we have near-stoichiometric UO_2[3,5,9,10] and ThO_2[6,7,9] permitting detailed analysis of their optical properties.

Few measurements of optical properties in the near-infrared to ultraviolet spectral region exist for UO_2: Schoenes studied reflectance from UO_2 single crystals in the range of 0.03 eV–13 eV and determined the complex-valued dielectric function, $\varepsilon = \varepsilon_1 + i\varepsilon_2$, from

numerical Kramers–Kronig integral calculations.[8] Meek *et al.* measured transmission of UO_2 thin films and determined the absorption properties.[11] He *et al.* used spectroscopic ellipsometry and density functional theory to explore the bandgap of uranium oxide thin films with various compositions.[12] Siekhaus and Crowhurst[13] and Dugan *et al.*[3] used spectroscopic ellipsometry to determine the critical-point structures in ε. Critical-point structures are associated with singularities in the joint density of states and caused by electronic band-to-band transitions.[14] Critical-point features have different shapes corresponding to the type of the band structure singularities and can be characterized by critical-point transition energy, broadening, and amplitude parameters. For UO_2, significant shifts were observed previously in the optical critical-point features obtained by reflectivity[8] and by ellipsometry.[3,13] No measurements of optical properties have been reported thus far for ThO_2.

Both uranium and thorium are similar with 6 valence electrons in uranium (electron configuration [Rn] 5f3 6d1 7s2) and 4 valence electrons in thorium ([Rn] 6d2 7s2). Their oxides are equivalent in structure, fluorite (cubic), and similar in unit cell dimensions. A comparison of the dielectric functions of single-crystal UO_2 and ThO_2 is now possible from analysis of spectroscopic ellipsometry measurements from the near-infrared to vacuum ultraviolet spectral region. We performed a critical-point analysis on the dielectric functions and compared the band-to-band transition parameters obtained from the analysis for the two actinide oxides.

In order to obtain meaningful physical information from spectroscopic ellipsometric data, appropriate physical models must be utilized for data analysis.[15] UO_2 and ThO_2 are both optically isotropic, and hence, it is assumed here that no polarization mode conversion between parallel (*p*) and perpendicular (*s*) occurs upon reflection of the light from the surfaces of the single crystals. The substrate-ambient boundary condition approximation was chosen, where the single-crystal actinides are considered as optically thick, quasihalf-infinite substrates.[16] Finite roughness at the single crystal–ambient interface affects the spectroscopic ellipsometry data and must be accounted for. Specifically, mechanically polished single crystal surfaces contain residual surface defect regions. An effective medium approximation was used to mimic the effects of physical surface roughness by an effective over-layer with effective dielectric function values and with effective thicknesses much smaller than the wavelengths.[16] Typically, the surface roughness layer thickness corresponds to the average physical roughness surface height variation.[17] Here, the dielectric function of the surface roughness layer was calculated by averaging ε of the actinide single crystal with void ($\varepsilon = 1$) with a variable volume ratio. The remaining model parameters are then the thickness of the surface roughness layer and the real and the imaginary parts of ε for every wavelength. Thus, a wavelength-by-wavelength regression analysis was utilized to determine all unknown parameters.

The optical critical-point features govern the spectral shape of the dielectric function of materials in the band-to-band transition spectral region. Critical-point structures can be rendered by model dielectric function approaches. The critical-point features are accounted for by 5 Gaussian-broadened oscillators, to render the imaginary part for each of their critical-point contribution, *n*,

$$\varepsilon_2(E) = \sum_{n=1}^{N} \mathrm{A}_n \left[e^{-\left(\frac{E-\mathrm{E}_n}{\sigma_n}\right)^2} - e^{-\left(\frac{E+\mathrm{E}_n}{\sigma_n}\right)^2} \right], \tag{1}$$

where

$$\sigma_n = \frac{\mathrm{B}_n}{2\sqrt{ln(2)}}, \tag{2}$$

and the real part of ε is obtained from Kramers–Kronig integration

$$\varepsilon_1(E) = \varepsilon_\infty + \frac{2}{\pi} P \int_0^\infty \frac{\xi \varepsilon_2(\xi)}{\xi^2 - E^2} d\xi. \tag{3}$$

Here, A_n, E_n, and B_n denote the *n*th-critical-point amplitude, transition energy, and transition broadening parameters, respectively. E is the photon energy, and ε_∞ is the static contribution to the dielectric function.[3,18]

The hydrothermal synthesis technique was used to grow ThO_2 and UO_2 single crystals for this study. Growth procedures for ThO_2 and UO_2 were quite similar in temperature, pressure, and mineralizer solution. The mineralizer solution for both growth reactions was a 6 M cesium fluoride solution (Alfa Aesar, 99.99%). Growth reactions were contained in sealed silver ampoules (99.95% Ag, Refining Systems Inc.) to minimize impurities that could be leached from the walls of the Inconel autoclave. These were sealed at either end via welding. For the ThO_2 sample, a seed crystal of ThO_2 was suspended in the upper portion of the silver tube on a silver seed rack. A charge of ThO_2 nutrient/feedstock (99.99% thorium oxide, International Bio-analytical Laboratories) was placed in the lower portion of the tube with a porous silver baffle separating the feedstock and the seed crystal. The baffle limits thermal mixing and ensures two distinct temperature regions in the tube. Once fully assembled, the silver tubes were placed in a 250 ml Inconel autoclave. Counter-pressure water was added to 80%–85% of the remaining volume to prevent the silver tube from rupturing due to pressure from the mineralizer solution.

Band heaters were placed on the autoclave to form two temperature zones that correspond to the feedstock and seed crystal zones. The cesium fluoride solution dissolves the feedstock at the higher temperature (dissolution) zone and forms a saturated solution. By adjusting the seed crystal (crystallization zone) to a lower temperature, a natural convective flow was established, thereby circulating the saturated solution to the cooler region. The lower temperature results in a supersaturated solution and ThO_2 is precipitated from solution onto the seed crystal. For ThO_2, the dissolution zone temperature was 650 °C and the crystallization zone was 600 °C, which generated a pressure of 172 MPa. These conditions were maintained for 90 days. Upon cooling, the ThO_2 seed crystal was extracted from the silver tube and rinsed to remove the residual cesium fluoride mineralizer. The UO_2 sample was also grown on a ThO_2 seed crystal, as no large UO_2 substrates/seeds were available. The mineralizer solution, temperatures, and pressures were exactly the same for the UO_2 (99.998% uranium oxide, International Bio-analytical Laboratories) growth procedure, although the growth was only maintained for 50 days.

Both samples were ground flat along the (100) crystallographic plane and polished. The samples were sonicated in both acetone and de-ionized water to remove residual crystal bond and loose particulates.

Lattice parameters for ThO_2 and UO_2 were obtained via single crystal X-ray diffraction (XtaLAB mini, Rigaku). Due to the excessive size of the ThO_2 and UO_2 crystals used in the ellipsometry measurements, lattice parameters could not be determined directly from these samples. Smaller spontaneously nucleated crystals of ThO_2 and UO_2

grown under similar conditions were used to measure the representative lattice parameters. For ThO_2, the lattice parameter was (5.6070 ± 0.0006) Å, which is consistent with the expected value of a = 559.7 pm.[19] The lattice parameters of UO_2 were observed in previous publications as (5.4703 ± 0.0006) Å corresponding to a stoichiometry of $UO_{2.003}$.[20,21] Further discussion and evidence supporting stoichiometric nature of these samples can be found in the supplementary material.

Spectroscopic ellipsometry data were collected from 0.75 eV to 6.4 eV with a dual-rotating compensator ellipsometer (RC2, J. A. Woollam Co., Inc.) as shown in Figs. 1 and 2. Data were acquired at seven angles of incidence ($\Phi_a = 45°, 50°, 55°, 60°, 65°, 70°$, and $75°$); however, while all are used in the data analysis, only three are shown for clarity. The spectral resolution from this instrument is 1 nm.

In the spectral range from 5 eV to 9 eV, data were collected with a nitrogen-purged rotating analyzer ellipsometer (VUV-VASE, J. A. Woollam Co., Inc.). In this region, data were acquired at three angles of incidence ($\Phi_a = 50°, 60°$, and $70°$). The resolution for this measurement was chosen to be 0.02 eV. Note also that although there is a significant overlap in the acquired data range, we show only data from 6.5 eV and above in Figs. 1 and 2 for clarity, with a dashed vertical line indicating the switch.

Figures 1 and 2 show experimental (symbols) and best-match model calculated (solid lines) spectroscopic ellipsometry data from multiple angles of incidence for the UO_2 and ThO_2 single crystals, respectively. We note excellent agreement between experimental data and model simulation data. The model simulation data were obtained by wavelength-by-wavelength determining ε and the surface roughness effective layer thickness. For the UO_2 crystal, we obtain a roughness effective layer thickness of approximately 4 nm, assuming that the roughness effective layer is formed from a 50:50 volume ratio of void and UO_2 material (dielectric function). For ThO_2, we obtain a roughness effective layer with a 10:90 volume ratio of void and ThO_2, with effective roughness layer thickness values of approximately 10 nm and 20 nm, differing between the VUV and RC2 measurements, respectively, which we identify as caused by surface effects due to the crystal polishing processes. The submicroscopic surface roughness also causes an angular spread of the reflected measurement beams, which enter the model analysis by considering the apertures of the two instruments. This modification of the model analysis consists of the consideration of a reflected beam with a spread over the angle of incidence which corresponds to the entrance pupil of the detector. This entrance is larger for the VUV instrument (approximately 8°) than for the near-IR–VIS instrument (approximately 3°). As a result, for the ThO_2 sample, a small offset is seen for the ellipsometry data across the spectral transition between the two instruments (Fig. 2). Note that this offset is purely instrumental and due to surface roughness, and both effects are thereby removed numerically as shown in the resulting dielectric function for ThO_2 in Fig. 4. Figures 3 and 4 depict the real

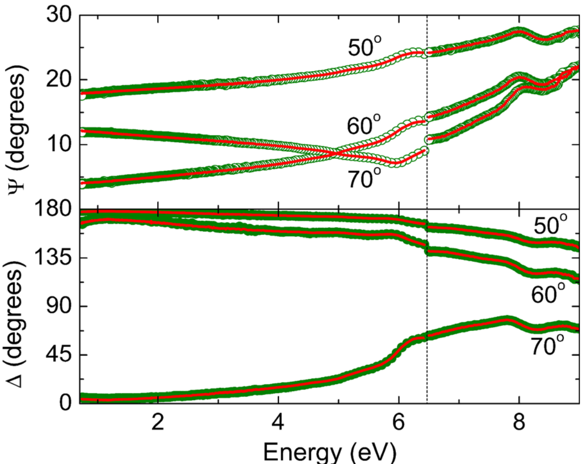

FIG. 2. Same as Fig. 1 for the ThO_2 single-crystal sample.

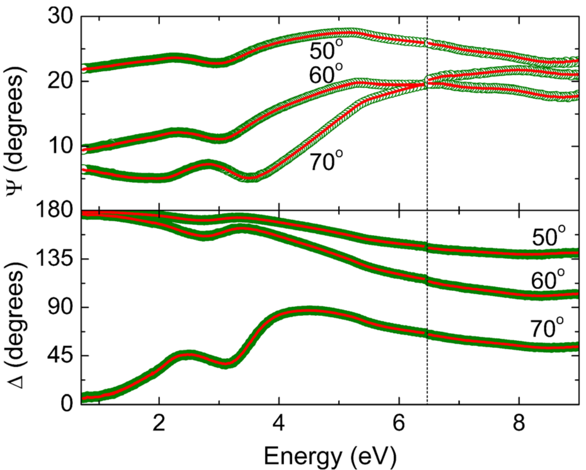

FIG. 1. Experimental (open symbols: Ψ, closed symbols: Δ) and best-match model calculated spectroscopic ellipsometry data (solid lines) for spectroscopic ellipsometry data measured at multiple angles of incidence for the UO_2 single crystal sample. The dashed vertical line indicates instrument switch at 6.5 eV.

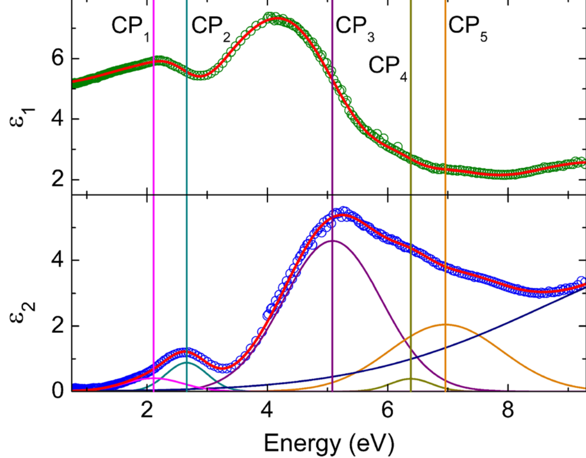

FIG. 3. Real (green symbols) and imaginary parts (blue symbols) of ε for the UO_2 single-crystal sample obtained from the wavelength-by-wavelength spectroscopic ellipsometry data analysis. Shown in comparison are the individual (solid lines) and total (red lines) critical-point transition contributions. Vertical lines indicate the individual critical-point transition energy parameters.

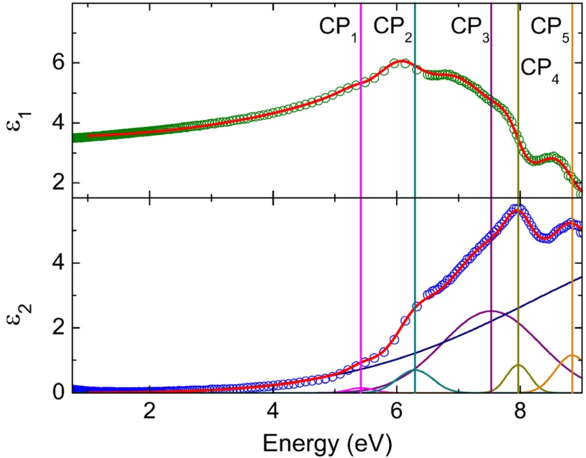

FIG. 4. Same as Fig. 3 for the ThO_2 single-crystal sample.

and imaginary parts of ε for UO_2 and ThO_2, respectively, obtained from our data analyses (symbols). For both samples, we observe a vanishing imaginary part of the dielectric response toward the near-infrared spectral range, indicative of a semiconductor material with nonvanishing bandgap energy. We observe a long tail-like feature in the ThO_2 dielectric function below the bandgap, indicative of the existence of crystalline defects within the ThO_2 sample.

Figures 3 and 4 also show the best-match model calculated critical-point contributions identified within our critical-point model analysis (solid lines). The individual critical-point contributions and their corresponding band-to-band transition center energy parameters are shown in the imaginary part of the dielectric functions with color coordinated vertical lines, in Figs. 3 and 4, thereby identifying the center energy, E_n, of each Gaussian oscillator rendering as close as possible the wavelength-by-wavelength determined functions ε for UO_2 and ThO_2, respectively. Table I and Table II list all critical-point parameter values within the investigated spectral range for the UO_2 single-crystal sample and for the ThO_2 single-crystal sample, respectively. We observe a large tail in the imaginary part of the dielectric function of ThO_2 below the bandgap which we model with a very broad Gaussian oscillator centered at higher energy outside the investigated spectral range. This oscillator also accounts for all higher energy transitions which contribute to the dielectric function and a similar oscillator

TABLE I. Critical-point parameters: amplitude (A_n), transition energy (E_n), and broadening (B_n) for the UO_2 dielectric function within the investigated spectral region. Digits in parentheses indicate the 90% confidence interval obtained from numerical best-match model analysis. A static contribution to the dielectric function near unity 1.02 ± 0.02 was found for the real part of the dielectric function of UO_2.

n	A_n (eV)	E_n (eV)	B_n (eV)
1	0.4 (0)	2. (1)	1. (1)
2	0. (8)	2.6 (6)	0.8 (0)
3	4.5 (9)	5.0 (8)	1.9 (3)
4	0.3 (9)	6.3 (9)	0.8 (1)
5	2.0 (4)	6.9 (6)	2.2 (1)

TABLE II. Same as Table I for ThO_2. A static contribution to the dielectric function of 1.01 ± 0.01 was determined for the real part of the dielectric function of ThO_2.

n	A_n (eV)	E_n (eV)	B_n (eV)
1	0.1 (2)	5.4 (4)	0.4 (3)
2	0.6 (7)	6.3 (5)	0.6 (6)
3	2.2 (3)	7.5 (0)	1.6 (3)
4	1.1 (8)	7.96 (5)	0.4 (5)
5	0.9 (9)	8.82 (6)	0.5 (9)

centered at higher energy was used in the UO_2 critical-point analysis as well.

The five distinct critical-point features in the optical response of both actinide oxides are enumerated on the order of ascending transition energy ($n = 1$, 2, 3, 4, and 5). These features are plotted using the same color codes in Figs. 3 and 4. In both cases, the 3rd ($n = 3$) critical-point features are the strongest contributions to the respective dielectric functions. As noted at the outset, while uranium and thorium have quite distinct configurations of valence electrons (uranium: [Rn] $5f^3\ 6d^1\ 7s^2$; thorium: [Rn] $6d^2\ 7s^2$), UO_2 and ThO_2 have many similarities, as is also evident from this work. Uranium's $5f$ electrons are not expected to participate in bonding and hence both actinide oxides crystallize in the same cubic fluorite structure, with only a slightly higher lattice constant for ThO_2.

The lowest critical-point transition energies, $E_{UO_2,1} = 2.1$ eV and $E_{ThO_2,1} = 5.4$ eV, are the fundamental band-to-band transition energy (bandgap energy) of the respective oxide. In spite of many similarities, it is clear that the critical-point features are sharper and more closely spaced for the wider bandgap material (ThO_2). This is expected for a wide bandgap oxide. In the case of UO_2, this experimentally determined lowest critical-point transition energy shows excellent agreement with the previously published results of band structure calculations, which predicted a bandgap energy of 2.19 eV.[3] Several studies have been conducted of the band structure of ThO_2.[22–24] The calculated values of the bandgap span a broad range of 3.3–6.9 eV. Our experimental value of 5.4 eV falls somewhere in the middle of this broad range but does not seem to match any specific published values.

In summary, high-quality, single-crystal actinide oxide samples of uranium oxide and thorium oxide were synthesized and investigated by structural and optical methods. A spectroscopic ellipsometry analysis determined the dielectric functions for both oxides, which reflect critical-point structures similar in appearance but shifted in photon energy. Five critical-point structures are observed in both materials, where the lowest bandgap energies of 2.1 eV are found for UO_2 and 5.4 eV for ThO_2. A strong blue shift by approximately 2–3 eV is obtained for all band-to-band transitions in ThO_2 with respect to UO_2.

See the supplementary material for details related to thoria and urania sample quality, stoichiometry, and electronic structure.

This work was supported in part by the National Science Foundation under Award No. DMR 1420645 (Nebraska Materials Research Science and Engineering Center) and under Award No. DMR 1808715. This work was supported in part by the Air Force Office of Scientific Research under Award No. FA9550-18-1-0360,

the Defense Threat Reduction Agency (Grant No. HDTRA1-14-1-0041), and the Domestic Nuclear Detection Office of the Department of Homeland Security (Grant No. HSHQDC14X00089). J.M.M. was supported by the Center for Thermal Energy Transport under Irradiation, an Energy Frontier Research Center funded by the U.S. Department of Energy, Office of Science, Office of Basic Energy Sciences. A.M., S.K., R.K., and M.S. acknowledge partial support from the J. A. Woollam Foundation. The authors thank Daniel Felker, Eric Hunt, J. W. McClory, T. D. Kelly, D. Turner, J. W. Kolis, and Xin Zhang for their assistance in taking XPS photoemission data shown within the supplementary material. The views expressed in this article are those of the authors and do not reflect the official policy or position of the United States Air Force, Department of Defense, or the U.S. Government.

REFERENCES

[1] T. T. Meek and B. von Roedern, Vacuum **83**, 226 (2008).
[2] C. Kruschwitz, S. Mukhopadhyay, D. Schwellenbach, T. Meek, B. Shaver, T. Cunningham, and J. Auxier, Proc. SPIE **9213**, 92130C (2014).
[3] C. L. Dugan, G. G. Peterson, A. Mock, C. Young, J. M. Mann, M. Nastasi, M. Schubert, L. Wang, W.-N. Mei, I. Tanabe, P. A. Dowben, and J. Petrosky, Eur. Phys. J. B **91**, 67 (2018).
[4] M. Mann, D. Thompson, K. Serivalsatit, T. M. Tritt, J. Ballato, and J. Kolis, Cryst. Growth Des. **10**, 2146 (2010).
[5] C. Young, J. Petrosky, J. M. Mann, E. M. Hunt, D. Turner, and P. A. Dowben, J. Phys.: Condens. Matter **29**, 035005 (2016).
[6] T. D. Kelly, J. C. Petrosky, J. McClory, T. Zens, D. Turner, J. M. Mann, J. Kolis, J. A. Colon Santana, and P. A. Dowben, in MRS Symposium Proceedings, 2013, Vol. 1576.
[7] T. Kelly, J. Petrosky, D. Turner, J. McClory, J. Mann, J. Kolis, X. Zhang, and P. A. Dowben, Phys. Status Solidi RRL **8**, 283 (2014).
[8] J. Schoenes, J. Appl. Phys. **49**, 1463 (1978).
[9] D. Turner, T. Kelly, G. Peterson, J. Reding, R. Hengehold, J. Mann, J. Kolis, X. Zhang, P. Dowben, and J. Petrosky, Phys. Status Solidi B **253**, 1970 (2016).
[10] C. Young, J. Petrosky, J. M. Mann, E. M. Hunt, D. Turner, and T. Kelly, Phys. Status Solidi RRL **10**, 687 (2016).
[11] T. Meek, B. Von Roedern, P. Clem, and R. Hanrahan, Jr., Mater. Lett. **59**, 1085 (2005).
[12] H. He, D. A. Andersson, D. D. Allred, and K. D. Rector, J. Phys. Chem. C **117**, 16540 (2013).
[13] W. Siekhaus and J. Crowhurst, in *IOP Conference Series: Materials Science and Engineering* (IOP Publishing, 2010), Vol. 9, p. 012055.
[14] P. Yu and M. Cardona, *Fundamentals of Semiconductors* (Springer, Berlin, Heidelberg, New York, 2005).
[15] H. Fujiwara, *Spectroscopic Ellipsometry* (John Wiley & Sons, New York, 2007).
[16] H. Fujiwara, *Spectroscopic Ellipsometry: principles and Applications* (John Wiley & Sons, 2007).
[17] G. E. Jellison, Thin Solid Films **313-314**, 33 (1998).
[18] M. Dressel and G. Grüner, *Electrodynamics of Solids* (Cambridge University Press, Cambridge, London, 2002).
[19] T. Yamashita, N. Nitani, T. Tsuji, and H. Inagaki, J. Nucl. Mater. **245**, 72 (1997).
[20] W. Young, L. Lynds, J. Mohl, and G. Libowitz, *An X-Ray and Density Study of Nonstoichiometry in Uranium Oxides* (Atomics International Divison of North American Aviation, Inc., Canoga Park, California, 1962).
[21] G. Leinders, T. Cardinaels, K. Binnemans, and M. Verwerft, J. Nucl. Mater. **459**, 135 (2015).
[22] T. Maehira and T. Hotta, J. Magn. Magn. Mater. **310**, 754 (2007).
[23] B. Szpunar and J. Szpunar, J. Nucl. Mater. **439**, 243 (2013).
[24] C. Mo, Y. Yang, W. Kang, and P. Zhang, Phys. Lett. A **380**, 1481 (2016).